

ARTICLE

Analogs of FTY720 inhibit TRPM7 but not S1PRs and exert multimodal anti-inflammatory effects

Gregory W. Busey¹ , Mohan C. Manjegowda¹ , Tao Huang¹ , Wesley H. lobst¹ , Shardul S. Naphade¹ , Joel A. Kennedy¹ , Catherine A. Doyle¹ , Philip V. Seegren¹ , Kevin R. Lynch¹ , and Bimal N. Desai^{1,2,3} 

TRPM7, a TRP channel with ion conductance and kinase activities, has emerged as an attractive drug target for immunomodulation. Reverse genetics and cell biological studies have already established a key role for TRPM7 in the inflammatory activation of macrophages. Advancing TRPM7 as a viable molecular target for immunomodulation requires selective TRPM7 inhibitors with *in vivo* tolerability and efficacy. Such inhibitors have the potential to interdict inflammatory cascades mediated by systemic and tissue-specialized macrophages. FTY720, an FDA-approved drug for multiple sclerosis inhibits TRPM7. However, FTY720 is a prodrug and its metabolite, FTY720-phosphate, is a potent agonist of sphingosine-1-phosphate (S1P) receptors. In this study, we test non-phosphorylatable FTY720 analogs, which are inert against S1PRs and well tolerated *in vivo*, for activity against TRPM7 and tissue bioavailability. Using patch clamp electrophysiology, we show that VPC01091.4 and AAL-149 block TRPM7 current at low micromolar concentrations. In culture, they act directly on macrophages to blunt LPS-induced inflammatory cytokine expression, though this likely occurs through multiple molecular targets. We found that VPC01091.4 has significant and rapid accumulation in the brain and lungs, along with direct anti-inflammatory action on alveolar macrophages and microglia. Finally, using a mouse model of endotoxemia, we show VPC01091.4 to be an efficacious anti-inflammatory agent that arrests systemic inflammation *in vivo*. Together, these findings identify novel small molecule inhibitors that allow TRPM7 channel inhibition independent of S1P receptor targeting which demonstrate potent, polymodal anti-inflammatory activities *ex vivo* and *in vivo*.

Introduction

Transient receptor potential melastatin-like 7 (TRPM7) is a member of the TRP superfamily of ion channels, a major class of drug targets (Koivisto et al., 2022; Moran, 2018). TRPM7 is one of two human channzymes encoding both a non-selective cation channel and an intracellular serine/threonine kinase domain (Nadler et al., 2001; Runnels et al., 2001). In utero, TRPM7 is broadly expressed in all tissues and is essential for embryogenesis. After embryogenesis, its expression subsides to low levels in most tissues but remains at relatively high levels in hematopoietic cells (Jin et al., 2008). In adult mice, post-embryonic deletion of *Trpm7* in various organs is well-tolerated after the completion of organogenesis (Jin et al., 2012), making TRPM7 a potential drug target for niche immunopharmacology. Since TRPM7 currents (I_{TRPM7} or simply I_M7) are readily detectable in immune cells, we explored and established significant functions of TRPM7 in both adaptive and innate immunity (Mendu et al., 2020). TRPM7 plays a salient role in macrophage activation in response to inflammatory stimuli, and accordingly, when *Trpm7* is deleted selectively in myeloid cells, the mice are highly resistant to endotoxemia (Schappe et al., 2018). *Trpm7*^{-/-} macrophages are

also defective in efferocytosis (Schappe et al., 2022), a process through which cell corpses are cleared, but they are normal in their ability to clear bacteria. Since microglia, the brain-resident macrophages, are crucial mediators of neuroinflammation, we reasoned that small molecule inhibitors of TRPM7 that accumulate in the brain may be of value in arresting neuroinflammation. Advancing this approach requires the identification of generally safe TRPM7 inhibitors that infiltrate the central nervous system.

TRPM7 assembles as homotetramers that are inhibited by $[Mg^{2+}]_i$ and can be observed electrophysiologically as a steep, outward-rectifying, cationic current in the plasma membrane (Duan et al., 2018; Nadezhdin et al., 2023). TRPM6 is a closely related channel that can form heterotetramers with TRPM7 (Chubanov et al., 2004), decreasing its sensitivity to physiological levels of $[Mg^{2+}]_i$ (Feroli et al., 2017). In contrast to the ubiquity of TRPM7, TRPM6 is primarily expressed in the kidneys and intestines (Groenestege et al., 2006) and nearly undetectable in macrophages (Heng et al., 2008). Consistently, deletion of *Trpm7* alone is sufficient to silence the outwardly rectifying, Mg^{2+} -inhibitable current typical of

¹Pharmacology Department, University of Virginia School of Medicine, Charlottesville, VA, USA; ²Carter Immunology Center, University of Virginia School of Medicine, Charlottesville, VA, USA; ³Cardiovascular Research Center, University of Virginia, Charlottesville, VA, USA.

Correspondence to Bimal N. Desai: bdesai@virginia.edu.

© 2023 Busey et al. This article is available under a Creative Commons License (Attribution 4.0 International, as described at <https://creativecommons.org/licenses/by/4.0/>).

I_{M7}/I_{M6} in macrophages (Schappe et al., 2022). In addition to its presence on the plasma membrane (PM), the bulk of the TRPM7 protein is found in intracellular vesicles termed M7-vesicles, or simply M7Vs (Abiria et al., 2017). The dynamics of TRPM7 membrane trafficking in macrophages have not been studied yet and the precise contributions of PM-resident and vesicular TRPM7 in macrophage functions are still a topic of investigation.

There are a number of reported TRPM7 inhibitors, but many lack specificity or potency, being repurposed drugs with greater activity at their primary targets (Chubanov et al., 2014, 2017). NS8593 and FTY720 (fingolimod) are such examples. NS8593 was originally developed as an inhibitor of small-conductance Ca^{2+} -activated K^+ (SK) channels (Strøbaek et al., 2006) but was later found to inhibit TRPM7 with an IC_{50} of 1.6 μM (Chubanov et al., 2012). However, NS8593 acts on SK-family channels with an IC_{50} in the range of 0.42–0.73 μM and has been shown to prolong the atrial action potential (Diness et al., 2010), limiting in vivo use. Waixeninic A, which is a natural compound isolated from marine soft coral, has been reported to inhibit TRPM7. This study claimed an IC_{50} of 16 nM, but this IC_{50} was derived in recording conditions that limit the development of TRPM7 currents. I_{TRPM7} is best resolved in Mg^{2+} -free conditions and in such conditions, the IC_{50} was shown to be 7 μM (Zierler et al., 2011). Moreover, inhibition of TRPM7 by 10 μM Waixeninic is very slow, taking up to 200 s to suppress I_{TRPM7} . Although Waixeninic has been used in vivo (Turlova et al., 2021; Sun et al., 2020), there are no pharmacokinetic studies proving that it is bioavailable in blood and tissues at concentrations needed to inhibit TRPM7. Until recently, this compound could only be derived from its natural sources and was not commercially available. However, there is now a viable total chemical synthesis (Steinborn et al., 2023) and this will facilitate further studies to clarify its utility in vivo. Despite these advances, there remains a need for chemically accessible TRPM7 inhibitors with pharmacological properties fit for targeting TRPM7 in preclinical in vivo studies. The present study focuses on improving FTY720 and molecules related to it, as they offer the key advantages of oral administration, low toxicity, and tissue bioavailability at concentrations that can inhibit TRPM7 effectively.

FTY720 is an immunosuppressive drug that is a structural analog of sphingosine and is currently used for the treatment of relapsing-remitting multiple sclerosis (Brinkmann et al., 2010). FTY720 is a prodrug that is phosphorylated in vivo by sphingosine kinases (SPHK1 and SPHK2) to yield the active immunosuppressant, FTY720-phosphate (FTY720-P; Paugh et al., 2003). FTY720-P is a picomolar (pM) agonist of multiple sphingosine-1-phosphate receptors (S1PRs), most prominently S1P1. Since supraphysiological agonism results in the effective downregulation of S1P1, FTY720 acts as a functional antagonist. In vivo, disruption of S1P1 signaling leads to lymph node sequestration of lymphocytes and concomitant lymphopenia (Brinkmann et al., 2002; Chiba et al., 1998; Matloubian et al., 2004). Interestingly, the non-phosphorylated form of FTY720 and sphingosine have no effect on S1PRs, but both were found to inhibit TRPM7 with IC_{50} s of 0.72 and 0.59 μM , respectively (Qin et al., 2013). Conversely, the phosphorylated form, FTY720-P, has no effect on I_{M7} . Prior pharmacokinetic studies of FTY720 have demonstrated that the

compound reaches tissue concentrations much higher than those observed in the blood, with lung tissue displaying the highest partition coefficient of all examined organs (Meno-Tetang et al., 2006). FTY720 has also been shown to cross the blood-brain barrier and accumulate in white matter at levels between 10- and 27-times that of the blood (Foster et al., 2007). We reasoned that non-phosphorylatable analogs of FTY720 could be candidates for more selectively inhibiting TRPM7 at the exclusion of S1PR targeting, and their likely tissue distribution would make them especially well-suited to in vivo neuropharmacology.

Although clinically efficacious, all S1P1 receptor agonists (four are marketed currently) cause initial-dose bradycardia in humans, a significant deleterious side effect that emerges from on-target S1P1 agonism (Camm et al., 2014). This species-specific effect was originally shown to be mediated by S1P3 agonism in mice (Sanna et al., 2004), which prompted a search for S1P1-selective FTY720 analogs. These efforts led to the discovery of molecules with conformationally constrained headgroups and preexisting chirality at their phosphorylation sites (Fig. S1; Lynch and Macdonald, 2006). While these medicinal chemistry efforts did not yield intended drug candidates (Albert et al., 2005), they yielded a set of well-characterized small molecules that proved useful for our study. We turned our attention to AAL-149 and VPC01091.4 which are non-phosphorylatable FTY720 analogs (Fig. 1) that are not active at S1P receptors, and, when administered to mice, do not evoke lymphopenia (Brinkmann et al., 2002; Zhu et al., 2007). In the process, we have identified VPC01091.4 as a potent inhibitor of TRPM7 ion channel activity. VPC01091.4 accumulates in the brain and lungs without evidence of toxicity, and in a mouse model of endotoxemia, it blunts systemic peripheral inflammation as well as neuroinflammation. An important caveat to these findings is that the anti-inflammatory effects of TRPM7 channel inhibitors (VCP4, AAL-149, FTY720, and NS8593) do not solely depend on TRPM7 as they are able to suppress LPS-induced IL-1 β expression even in TRPM7 KO bone marrow-derived macrophages (BMDMs). The ability of these drugs to suppress IL-6 expression appears more dependent on intact TRPM7, but these differential effects strongly hint at multiple inflammatory mediators being targeted by these compounds. Nonetheless, VPC01091.4 represents a significant improvement in selectivity over FTY720, as it allows attempts at in vivo targeting of TRPM7 without driving lymphopenia, a typical result of S1PR targeting. Future work may identify more potent and selective TRPM7 inhibitors within the space of non-phosphorylatable sphingosine isomers.

Materials and methods

Resource availability

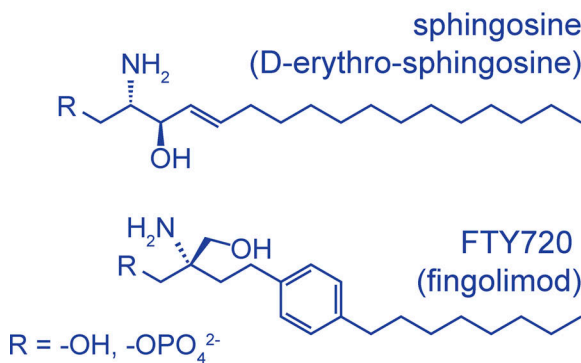
Materials availability

All unique/stable reagents generated in this study are available from the corresponding author with a completed Materials Transfer Agreement.

Cell culture

All cells were cultured at 37°C with 5% CO₂. HEK 293T cells (CRL-3216; ATCC), HeLa cells (CCL-2; ATCC), RAW 264.7

A Phosphorylatable Isomers



B Non-Phosphorylatable Isomers

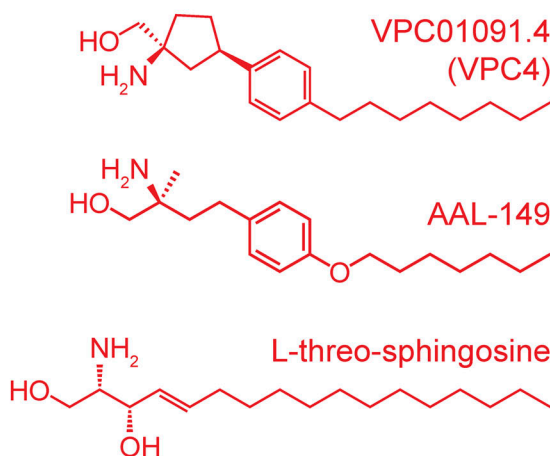


Figure 1. Structure of sphingosine analogs that inhibit I_{TRPM7} . (A) The structure of the predominant, naturally occurring sphingosine isomer (D-erythro-sphingosine or sphingosine) and FTY720 (fingolimod) are shown. Both sphingosine and FTY720 inhibit I_{M7} but they are phosphorylated in vivo, and the phospho-analogs are potent agonists of the ubiquitous S1P1 receptor. FTY720 is a prochiral molecule, only the S enantiomer (shown) is produced by sphingosine kinases. Phosphorylatable isomers are shown in blue. (B) VPC01091.4, AAL-149, and L-threo-sphingosine are structural analogs of sphingosine that are not phosphorylated in vivo and lack activity against S1PRs. The existing stereochemistry of these compounds places their hydroxymethyl groups in a position that is not amenable to phosphorylation by sphingosine kinases.

macrophages (TIB-71; ATCC), and BV-2 microglial cells (ABC-TC212S; AcceGen Biotech) were cultured in DMEM (11995065; Gibco) with 10% fetal bovine serum (FBS; Avantor Seradigm Premium Grade Fetal Bovine Serum 97068-085). FBS was heat-inactivated prior to use at 56°C for 30 min. BMDMs were isolated and cultured as previously described (Schappe et al., 2018) and differentiated into mature macrophages over 7 d through culture in BMDM media (RPMI 1640, 10% FBS, and 20% L-929 culture supernatant; Gibco).

Alveolar macrophages were isolated and cultured from wildtype (WT) C57BL/6 mice (Strain #000664; Jackson Laboratory) using an established protocol (Nayak et al., 2018). Briefly, euthanized mice were perfused with 10 ml of ice-cold

PBS through the right ventricle until the lung tissue exhibited a pale-white appearance. A 22G catheter was then inserted into the trachea immediately superior to the larynx and affixed in place using a sterile suture around the trachea. Using a 5-ml syringe filled with 3 ml of bronchoalveolar lavage buffer (“BAL buffer”: Ca^{2+} - and Mg^{2+} -free PBS + 1 mM EDTA), the lungs were first filled with ~2 ml of BAL buffer, then flushed five times in a cycle involving the installation and removal of 1 ml of buffer. The collected BAL fluid was pooled and the cyclical perfusion step was repeated with fresh buffer until a total of ~10 ml of BAL fluid was collected. BAL fluid with gross evidence of blood contamination was discarded. A pellet was obtained through centrifugation at $500 \times g$ for 5 min, and contaminating red blood cells were lysed by resuspending cells for 5 min in 5 ml of ice-cold ACK Lysis buffer (A1049201; Gibco). The cells were then pelleted at $500 \times g$ for 5 min, resuspended in alveolar macrophage culture media (DMEM supplemented with 10% FBS, 20% L-929 culture supernatant, 1 mM sodium pyruvate, 10 mM HEPES, and 1× penicillin/streptomycin), and plated onto untreated tissue culture dishes for 24 h. The media was exchanged prior to use to remove unattached cells.

To overexpress TRPM7, HEK 293T cells were plated at a density of 500,000 cells per well (day 0), transfected at 80–90% confluence (day 1), and were patched 24–36 h after transfection (day 2). TRPM7 overexpression was performed using WT mouse TRPM7 (2.5 μ g plasmid DNA; Desai et al., 2012) and jetOPTIMUS DNA Transfection Reagent (101000006; Polyplus). To enhance the selection rate of TRPM7-overexpressing cells, eGFP (#22152; Addgene) was included at a 1:10 dilution (0.25 μ g) and only GFP-positive cells were patched. The observed overexpression current displayed the characteristic outward rectification, run-up, and reversal potential of I_{TRPM7} and was inhibited by 10 mM $MgCl_2$ and 5 μ M FTY720.

All cells were cultured at 37°C with 5% CO_2 . HEK 293T cells (CRL-3216; ATCC), HeLa cells (CCL-2; ATCC), RAW 264.7 macrophages (TIB-71; ATCC), and BV-2 microglial cells (ABC-TC212S; AcceGen Biotech) were cultured in DMEM (11995065; Gibco) with 10% FBS (Avantor Seradigm Premium Grade Fetal Bovine Serum 97068-085). All cell lines were negative for mycoplasma contamination as confirmed using a MycoStrip Mycoplasma Detection Kit (rep-mys-10; InvivoGen). FBS was heat-inactivated prior to use at 56°C for 30 min. BMDMs were isolated and cultured as previously described (Schappe et al., 2018) and differentiated into mature macrophages over 7 d through culture in BMDM media (RPMI 1640, 10% FBS, and 20% L-929 culture supernatant; Gibco).

Test compounds

VPC01091.1 [((*IR*,*3S*)-1-amino-3-(4-octylphenyl)cyclopentyl)methanol] is commercially available (Avanti Polar Lipids, 857345). VPC01091.2-P [((*IS*,*3S*)-1-amino-3-(4-octylphenyl)cyclopentyl)methyl dihydrogen phosphate], VPC01091.3 [((*IR*,*3R*)-1-amino-3-(4-octylphenyl)cyclopentyl)methanol], VPC01091.4 [((*IS*,*3R*)-1-amino-3-(4-octylphenyl)cyclopentyl)methanol], and AAL-149 ((*2S*)-2-amino-4-(4-heptoxyphenyl)-2-methylbutan-1-ol) were generously provided by Dr. Kevin R. Lynch (University of Virginia). FTY720 (fingolimod), L-threo-sphingosine, and NS8593 were

purchased from Cayman Chemical (item #10006292, #10010541, and #29774, respectively). AAL-149 was solubilized in 100% ethanol, and all other compounds were solubilized in DMSO.

Patch clamp electrophysiology

Whole-cell patch clamp electrophysiology was performed as described previously (Schappe et al., 2022). Briefly, the external solution contained (in mM) 140 Na-methanesulfonate, 5 Cs-gluconate, 2.5 CaCl₂, and 10 HEPES, pH 7.4 (adjusted with NaOH), at an osmolality of 280–290 mOsm/kg. The internal pipette solution contained (in mM) 115 Cs-gluconate, 3 NaCl, 0.75 CaCl₂, 10 HEPES, 10 HEDTA, 1.8 Cs₄-BAPTA, and 2 Na₂ATP, pH 7.3 (adjusted with CsOH), at an osmolality of 273 mOsm/kg. Intracellular free [Ca²⁺] was estimated to be ~100 nM using the online WEBMAXC standard calculator at <https://somapp.ucdmc.ucdavis.edu/pharmacology/bers/maxchelator/webmaxc/webmaxcS.htm> (Bers et al., 2010). Recordings were captured in pCLAMP 9 (Molecular Devices) using a 400-ms ramp protocol from -100 to +100 mV and a holding potential of 0 mV. Sampling was performed at 10 kHz with a 5 kHz low-pass band filter using an Axopatch 200B amplifier (Molecular Devices). All electrophysiology experiments were conducted at RT (~23°C). Because I_{M7} exhibits a strong flow-induced transient increase in current (Oancea et al., 2006), the maximum current is taken as the stable maximum current observed prior to the perfusion of the next solution. Similarly, the minimum current for each inhibitor dose is taken as the stable minimum current observed after the drug has had time to exert an effect and after the flow-driven transient increase has subsided.

LDH-release cytotoxicity assay

WT HeLa cells were plated at a density of 10,000 cells per well into a 96-well tissue culture microplate (3610; Costar). AAL-149, VPC01091.4, or vehicle at 0.1, 1, 5, 10, and 25 μM was added to cells with media for a final volume of 100 μl and incubated for 24 h. LDH release was quantified using a CyQUANT LDH Cytotoxicity Assay (C20300; Thermo Fisher Scientific) and a Flex-Station 3 plate reader using SoftMax Pro 7 (Molecular Devices).

In vitro LPS-induced inflammation experiments

RAW 264.7 macrophages or BMDMs were seeded at a density of 250,000 cells per well into a 12-well tissue culture plate in 1 ml of media and left to incubate overnight. The indicated drug or vehicle control was added to each well, and the plate was agitated and left to incubate for 10 min. The cells were then treated with LPS (1 μg/ml) or an equivalent volume of PBS, agitated, and left to incubate for 3 h. Cells were washed with PBS and then RNA isolation was performed using RNeasy Plus Micro Kit (74134; Qiagen). cDNA was produced using GoScript Reverse Transcriptase (A5004; Promega) and a quantitative PCR was performed using SensiFast SYBR (98020; Bioline) and Bio-Rad CFX Connect thermocycler. Each datum represents an individual, biological replicate that is the mean of duplicate technical replicates. Fold-changes are all reported relative to untreated controls for each experiment and were calculated using the ΔΔC_t method, with β₂-microglobulin used as the housekeeping gene for each sample. The experiment was performed similarly with

BV-2 microglia and alveolar macrophages, except that cells were plated at a density of 100,000 cells per well into a 24-well tissue culture plate with 1 ml of media per well.

In vivo LPS-induced peritonitis mouse model

12-wk-old WT C57BL/6J mice were purchased from Jackson Laboratory (Strain #000664). An equal number of male and female mice were randomly assigned to each treatment group. All studies were conducted according to a protocol approved by the University of Virginia Animal Care and Use Committee. Mice were socially housed with littermate controls and provided with free access to a standard chow diet and water. Baseline weights were taken <1 h prior to the experiment for individual dose calculations. For the sublethal model, mice were injected intraperitoneally with LPS (1 mg/kg), VPC01091.4 (30 mg/kg), both LPS and VPC01091.4, or vehicle alone (20% 2-hydroxypropyl-β-cyclodextrin in PBS). The volume injected was 200 μl and solutions were sterile-filtered (0.45 μm) prior to use. Mice were observed for 4 h, with weight and symptoms assessed every 2 h (t = 0, 2, and 4 h). Mice were euthanized at 4 h, then blood was collected via cardiac puncture and anticoagulated with K₂EDTA. The inferior vena cava was severed immediately superior to the common iliac bifurcation, and the mice were perfused using 10 ml of ice-cold PBS into each cardiac ventricle. The lungs were dissected, coarsely homogenized, and partitioned into separate samples for RNA extraction and mass spectrometry analysis. Samples to be used for RNA were stored at -20°C in RNAlater Stabilization Solution (AM7021; Thermo Fisher Scientific) while samples for use in mass spectrometry were flash-frozen in liquid nitrogen. Whole brains were physically dissected, coarsely homogenized, and stored for later processing as with the lung tissue. 10 μl of each whole blood sample was reserved for mass spectrometry analysis, 15 μl was used to obtain lymphocyte counts with a Hematology Analyzer (Heska Element HT5), and the remainder was used to produce plasma through centrifugation at 2,000 × g for 15 min at 4°C. Plasma cytokines were then measured using a multiplex mouse proinflammatory cytokine panel performed by the University of Virginia Flow Cytometry Core (RRID: SCR_017829). Cytokine values beyond the limit of detection (LOD) are reported as the LOD value. Tissue RNA was isolated from preserved samples using 30 min of automated homogenization at 30 Hz with 5-mm ball-bearings in RLT Plus Lysis Buffer (TissueLyser II; Qiagen); RNA was then isolated using a RNeasy Plus Micro Kit (74134; Qiagen). Whole-tissue cytokine expression changes were then measured using qRT-PCR as with ex vivo cell culture experiments. For the lethal dose model, mice were injected with LPS (25 mg/kg), both LPS and VPC01091.4, or vehicle alone (20% 2-hydroxypropyl-β-cyclodextrin in PBS). Symptoms were scored according to a standardized clinical score sheet that assessed conjunctivitis, lethargy, degradation in hair grooming behavior, stool changes, and facial grimace (Table 1). Mice that lost >20% of their starting body weight or received a clinical score of 8 or greater were euthanized.

LC-MS/MS sample preparation

The sample preparation method was adapted from that published by Shaner et al. (2009). Specifically, homogenized tissue

Table 1. Scoring sheet for humane endpoints: LPS-induced peritonitis model

Scoring parameter	0	1	2
Conjunctivitis	Normal	Single eye open with visible discharge	Eyes closed with discharge and swelling
Lethargy	Normal locomotion and reaction, >3 steps	Inactive, <3 steps after moderate stimulation, slight hunching Score as 2 for this category	Only lifting of head after moderate stimulation <1 step, severe hunching Score as 4 for this category
Hair coat	Well-groomed with smooth coat	Rough coat, minor ruffling	Unkempt fur, dull coat
Grimace pain	Normal	Moderate orbital tightening or nose bulge	Severe orbital tightening, nose bulge, and collapsed ear position
Stool	Normal	Creamy consistency	Watery diarrhea

Animals receiving a total score ≥ 8 or those which have lost 20% of more of their body weight will be euthanized.

(100 μ l) was added to a mixture of methanol and chloroform (2 ml, 3:1, LCMS grade) and incubated at 48°C for 16 h. The mixture was cooled to room temperature, an alcoholic KOH solution (200 μ l, 1 M in LCMS-grade methanol) was added, and the mixture was further incubated at 37°C for 2 h. The samples were neutralized with glacial acetic acid (20 μ l) and centrifuged at 4°C for 10 min at 10,000 $\times g$. The supernatant fluid was transferred to a glass vial and dried under a stream of nitrogen. The material was dissolved in LCMS grade methanol (500 μ l), vortexed, and centrifuged at 4°C for 10 min at 10,000 $\times g$. The supernatant fluid was transferred to LC vials for analysis by LC-MS/MS.

LC-MS/MS analysis

Analyses were performed using a tandem quadrupole mass spectrometer (Xevo TQ-S micro; Waters) coupled to a UPLC (Waters Acquity h-class+) inlet equipped with a reverse phase C18 UPLC column (BEH C-18 1.7 μ m bead size, 2.1 \times 50 mm; Waters). The method used is a modification of that published by Frej et al. (2015). Specifically, the LC flow rate was set at 0.4 ml/min and the column temperature was 60°C. Mobile phase A consisted of water:methanol:formic acid (79:20:1) while mobile phase B was methanol:acetone:water:formic acid (68:29:2:1). The run began with 50:50 A:B for 0.5 min. Solvent B was then increased linearly to 100% B in 3.5 min and held at 100% B for 3 min. The column was re-equilibrated to 50:50 A:B for 1.5 min. A volume of 3 μ l was injected into the column. Both VPC01091.4 and FTY720 were analyzed in positive mode using MRM protocols as follows: VPC01091.4 (304.2 \rightarrow 269.2, voltages: cone 48, collision 12) and FTY720 (308.2 \rightarrow 255.2, voltages: cone 4, collision 14). Quantification was accomplished using Waters TargetLynx ver. 1.4. The concentration of VPC01091.4 in tissues was calculated using the metric ratio to the internal standard (FTY720) and normalized to wet tissue weights.

Statistics and data processing

Data were analyzed using Microsoft Excel, Prism 9.5 (GraphPad Software), and Origin Pro 7.5 (OriginLab). Chemical structures were created using ChemDraw Professional 20.1.1 (Perkin-Elmer). Electrophysiology traces were plotted using Origin Pro

7.5, and the remaining data were plotted and statistically tested using Prism. Outliers were determined using the robust regression and outlier removal (ROUT) function within Prism. IC₅₀ values were determined by plotting the percentage of maximum current observed as a function of applied drug concentration. A non-linear regression was fit using a standard Hill slope of -1.0 and the model: $Y = 100 / \left[1 + \left(\frac{[Inhibitor]}{IC_{50}} \right)^H \right]$. Where appropriate, data are presented as individual values; otherwise the sample sizes and precision measures are indicated in the figure legends. P values of <0.05 were considered statistically significant.

Online supplemental material

Fig. S1 shows the stereoisomers of sphingosine, VPC01091, and AAL-149. Fig. S2 shows the electrophysiology recording setup, analysis method, and peak TRPM7 current density at +100 mV versus time graphs for VPC01091 stereoisomers, AAL-149, and L-threo-sphingosine.

Results

Identification of VPC01091 stereoisomers that block I_{M7}

VPC01091 has four stereoisomers (denoted VPC01091.1–4). Isomers 2 and 4 were of primary interest to us because they are not substrates of sphingosine kinases (Fig. S1 B). We carried out whole-cell patch clamp electrophysiology on HEK 293T cells overexpressing mouse TRPM7 and isolated the typical outwardly rectifying I_{M7} reversing at 0 mV. I_{M7} is inhibited by free Mg²⁺ and, consequently, I_{M7} is revealed using a pipette solution rich in divalent chelators that deplete free [Mg²⁺]_i. When applied to maximal I_{M7}, VPC01091.4 resulted in significant inhibition (Fig. 2 A, top). VPC01091.1 and VPC01091.3 also inhibited I_{M7} (Fig. 2, D and F). VPC01091.2 was not available for testing, but predictably, the application of its chemically phosphorylated variant, VPC01091.2-P, had a negligible effect on peak I_{M7} (Fig. 2 E). Next, by carrying out dose-response studies, we determined the IC₅₀ of VPC01091.4 to be 0.665 μ M for TRPM7 inhibition (Fig. 2 A, bottom). Henceforth, we refer to VPC01091.4 as simply VPC4.

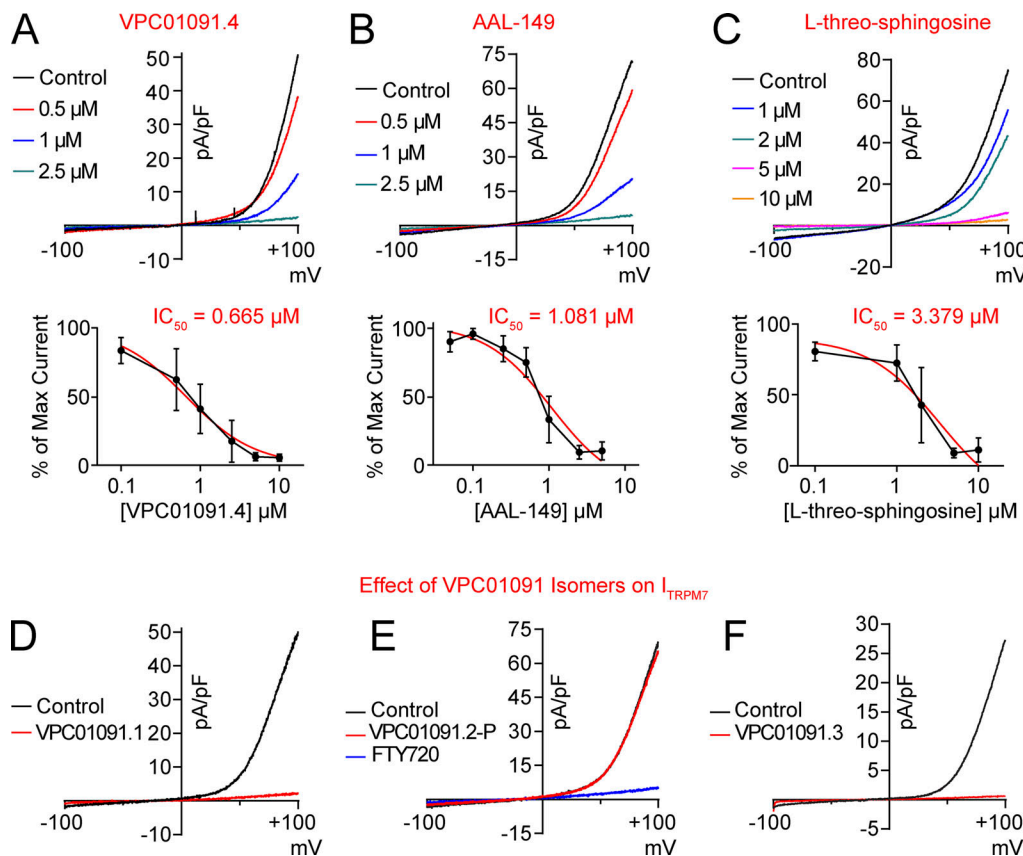


Figure 2. VPC01091.4, AAL-149, and L-threo-sphingosine inhibit TRPM7 current. The effects of sphingosine analogs on whole-cell TRPM7 currents from HEK 293T cells overexpressing mouse TRPM7 are shown. Peak current traces (black) represent the maximal current observed at +100 mV after allowing for I_{M7} to run-up in control bath solution and drug-treated traces represent the minimal current observed after drug application. **(A-C)** Representative recordings show the dose-dependent inhibition of I_{M7} by VPC01091.4, AAL-149, and L-threo-sphingosine. **(A)** Top: Dose-dependent inhibition by VPC01091.4 of maximal TRPM7 currents. Bottom: IC_{50} was determined to be 0.665 μM by best fit non-linear regression model (red trace; 95% CI $IC_{50} = 0.525$ to 0.834, $n = 8$ for each condition, SEM are shown). **(B)** Top: Dose-dependent inhibition of I_{M7} by AAL-149. Bottom: IC_{50} was determined to be 1.081 μM (95% CI $IC_{50} = 0.656$ –1.866, $n = 3$ at 0.1 μM , and $n \geq 5$ for all other conditions, SEM are shown). **(C)** Top: Dose-dependent inhibition of I_{M7} by L-threo-sphingosine. Bottom: IC_{50} was determined to be 3.379 μM (95% CI $IC_{50} = 1.169$ –14.940, $n = 2$ at 10 μM , and $n \geq 3$ for all other conditions, SEM are shown). **(D-F)** The effects of VPC01091 stereoisomers on whole-cell TRPM7 currents from HEK 293T cells overexpressing mTRPM7 are shown. Example traces from cells treated with 10 μM VPC01091.1 (D) or VPC01091.3 (F). VPC01091.2 was not available to be tested, but the chemically phosphorylated VPC01091.2-P had no effect on I_{M7} (E), consistent with the observation that S1P and FTY720-P do not inhibit I_{M7} . Subsequent application of 5 μM FTY720 was able to inhibit I_{M7} .

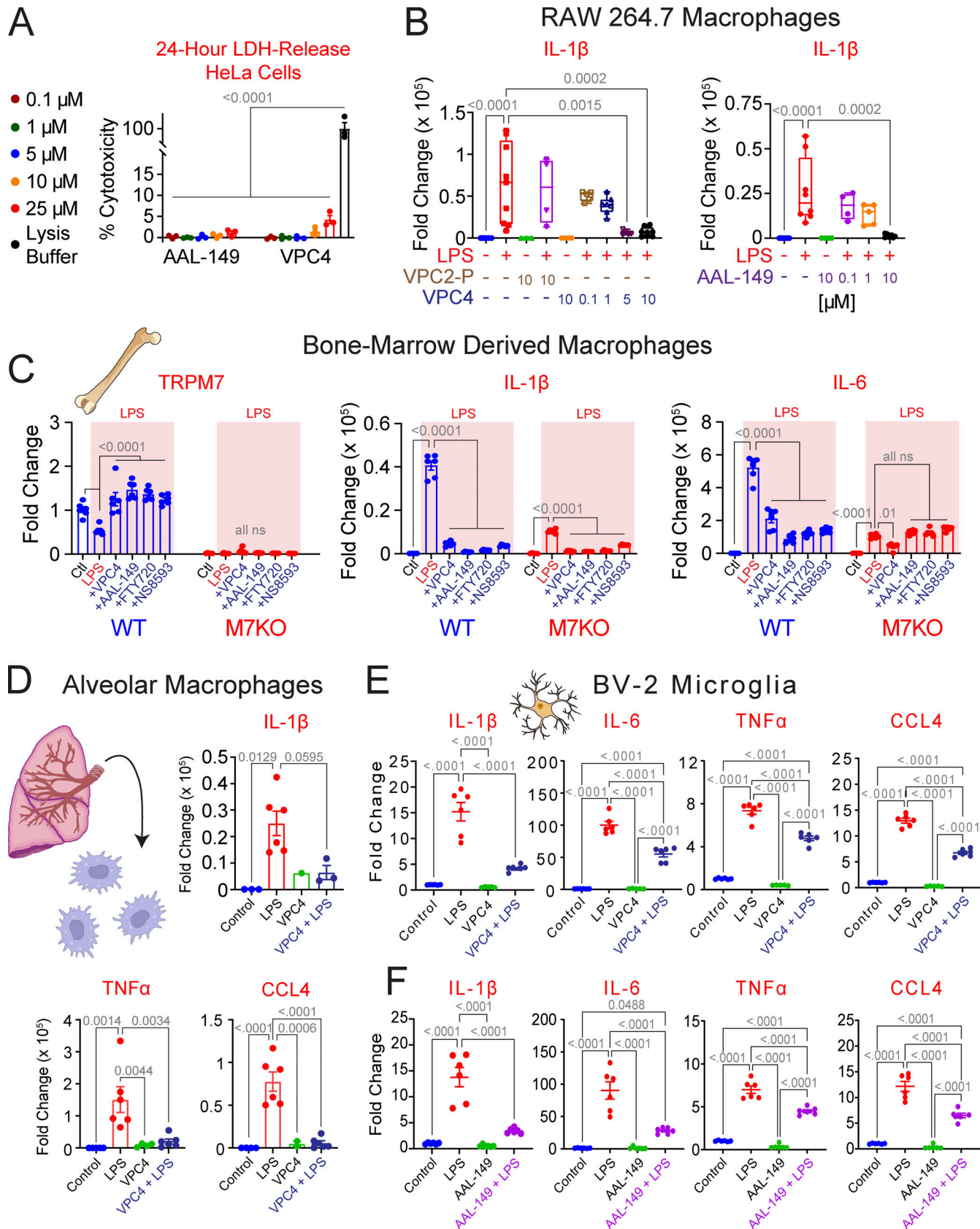
AAL-149 and L-threo-sphingosine are additional blockers of I_{TRPM7}

Next, we evaluated an additional sphingosine-like compound, AAL-149, which is the non-phosphorylatable enantiomer of AAL-151 (Fig. S1 C). AAL-149 also inhibited I_{M7} in a dose-dependent manner, with a calculated IC_{50} of 1.081 μM (Fig. 2 B). VPC4 and AAL-149 thus represent drug candidates with similar potency against TRPM7 as FTY720 ($IC_{50} = 0.72 \mu M$). However, these proprietary compounds are not commercially available. For that reason, we also attempted to identify a more widely available analog of sphingosine that cannot be phosphorylated. “Sphingosine” or D-erythro-sphingosine (2S,3R), is one of four possible stereoisomers and the predominant naturally occurring isomer (Merrill, 2002). We took advantage of the observation that while the erythro-enantiomers are phosphorylated by mammalian sphingosine kinases, the threo-enantiomers are competitive inhibitors of sphingosine kinases and not appreciably phosphorylated in vivo (Buehrer

and Bell, 1992). We tested a commercially available L-threo-(2S,3S)-sphingosine for its potential to inhibit I_{M7} (Fig. 1 B). We found that L-threo-sphingosine inhibits TRPM7 current (Figs. 2 and S2) with a reduced potency in comparison to VPC4, AAL-149, and FTY720. The calculated IC_{50} was 3.379 μM . Due to the reduced potency of L-threo-sphingosine, for further studies we focused on VPC4 and AAL-149.

VPC4 and AAL-149 are not cytotoxic at concentrations necessary to inhibit I_{M7}

To test whether VPC4 and AAL-149 could be tolerated at effective inhibitory doses, we incubated HeLa cells for 24 h with a range of compound concentrations and measured LDH release as a readout of cytotoxicity (Fig. 3 A). For both VPC4 and AAL-149, dosages up to 10 μM did not result in any significant cytotoxicity. At the highest dose of 25 μM , which is >30 times its IC_{50} , VPC4-treated cells exhibited modest cytotoxicity (4% compared with positive control of 100% cytotoxicity). These findings



Downloaded from https://academic.oup.com/jgp/article-pdf/156/1/jgp.20231341/1977/jgp-20231341.pdf by guest on 10 February 2026

Figure 3. VPC01091.4 and AAL-149 suppress LPS-induced inflammation in macrophages and microglia. (A) HeLa cells display minimal cytotoxicity to AAL-149 and VPC01091.4 at doses up to 25 μ M (mean cytotoxicity <5% for each condition, $n = 3$ for each dose). $P < 0.0001$ for all comparisons relative to lysis control. **(B)** Change in IL-1 β expression observed by qRT-PCR in RAW 264.7 macrophages following stimulation with LPS (1 μ g/ml for 3 h). Pretreatment with

≥ 5 μ M of VPC01091.4 or 10 μ M AAL-149, but not VPC01091.2-P, significantly reduced LPS-stimulated *IL-1 β* expression. For brevity, only statistically significant comparisons from the LPS-only treated groups are shown. Box and whisker plots display the minimum, first quartile, median, third quartile, and maximum values. **(C)** BMDMs from WT (*Trpm7 $^{fl/fl}$*) and TRPM7 KO (*Trpm7 $^{fl/fl}$ LysM Cre*) mice were isolated and differentiated for 7 d prior to use for an LPS-induced inflammation assay. Expression levels of *Trpm7*, *IL-1 β* , and *IL-6* as measured by qRT-PCR are displayed. Levels of TRPM7 expression are normalized to control-treated WT BMDMs, and *IL-1 β* , and *IL-6* expression levels are normalized to control-treated BMDMs for their respective genotype. Four different TRPM7 inhibitors were used: 10 μ M VPC4, 10 μ M AAL-149, 5 μ M FTY720, or 30 μ M NS8593. Statistical analysis was performed using a two-way ANOVA with Tukey's multiple comparison within each genotype. **(D)** Alveolar macrophages isolated from WT mice were stimulated with LPS as above. Pretreatment with 10 μ M VPC4 significantly suppressed the expression of *IL-1 β* , *TNF α* , and *CCL4*. **(E and F)** Inflammatory cytokine expression levels as measured by qRT-PCR in cultured BV-2 microglia pretreated with vehicle, 10 μ M VPC01091.4 (E), or 10 μ M AAL-149 (F) before stimulation with LPS (1 μ g/ml for 3 h). Unless stated otherwise, ordinary one-way ANOVA was used for analyses, and error bars represent SEM. The vehicle used for VPC4, VPC2-P, FTY720, and NS8593 was DMSO, and the vehicle for AAL-149 was 100% ethyl alcohol (<0.2% vol/vol in experimental media for each). VPC4 = VPC01091.4 and VPC2-P = VPC01091.2-P.

establish VPC4 and AAL-149 as viable alternatives to FTY-720 for cell-based investigations of TRPM7, with the key advantage that they do not act on S1P receptors (Brinkmann et al., 2002; Zhu et al., 2007).

VPC4 and AAL-149 inhibit LPS-induced inflammatory gene expression in macrophages and microglia

We have previously shown that *Trpm7 $^{fl/fl}$* macrophages exhibit significantly reduced inflammatory gene expression in response to LPS and other TLR ligands (Schappe et al., 2018). Based on the use of FTY720, we also concluded that the ion channel activity of TRPM7 was paramount for its function in inflammatory signaling but acknowledged the caveat that at the concentrations used, FTY720 would clearly target the macrophage S1PRs. We therefore tested whether VPC4 and AAL-149 can inhibit macrophage activation in response to LPS. RAW 264.7 macrophages were pretreated with either VPC4, VPC01091.2-P, or AAL-149, prior to exposure to LPS (1 μ g/ml for 3 h; Fig. 3 B). Macrophages stimulated with LPS displayed a significant upregulation in *IL-1 β* expression relative to unstimulated macrophages. When pretreated with VPC01091.2-P, which does not inhibit TRPM7, there was no significant inhibition of *IL-1 β* gene expression. However, in cells pretreated with VPC4, the gene expression of *IL-1 β* was almost completely abrogated at 5 and 10 μ M. Similarly, pretreatment with AAL-149 (10 μ M) also completely abrogated *IL-1 β* gene expression in response to LPS.

Next, we sought to evaluate the TRPM7-dependent anti-inflammatory effects of VPC4 and AAL-149 and compare them to the widely used TRPM7 inhibitors FTY720 and NS8593. (Fig. 3 C). BMDMs from WT (*Trpm7 $^{fl/fl}$*) and TRPM7 KO (*Trpm7 $^{fl/fl}$ LysM Cre*) mice were isolated and differentiated for 7 d prior to use for an LPS-induced inflammation assay. TRPM7 KO BMDMs had a near total loss of *Trpm7* expression relative to WT cells (Fig. 3 C, left). Interestingly, WT BMDMs demonstrated a significant reduction in *Trpm7* expression after treatment with LPS, and this effect was prevented with the treatment of any of the four tested TRPM7 inhibitors. Next, we observed that LPS-stimulated expression of *IL-1 β* and *IL-6* was greatly reduced in the TRPM7 KO BMDMs relative to WT. In *Trpm7* KO BMDMs, *IL-6* expression was suppressed to similar degrees both genetically and pharmacologically, with the exception of VPC4 treatment, where an additive effect was observed (Fig. 3 C, right). In both TRPM7 WT and KO BMDMs, *IL-1 β* expression was suppressed through treatment with the TRPM7 inhibitors (Fig. 3 C, middle). Taken together, these data indicate that some LPS-

induced inflammation may be driven in a TRPM7-dependent manner (such as for *IL-6*), but the ability for *IL-1 β* expression to be suppressed pharmacologically in TRPM7 KO BMDMs indicates off-target effects of these compounds that are independent of TRPM7.

Lastly, we observed that VPC4 exhibited direct anti-inflammatory effects upon primary mouse alveolar macrophages (Fig. 3 D) and the mouse BV-2 microglial cell line (Fig. 3 E). AAL-149 also exerted similar anti-inflammatory effects (Fig. 3 F). These results establish VPC4 and AAL-149 as small-molecule drugs that exert potent anti-inflammatory effects in several macrophage subtypes.

VPC4 reduces systemic peripheral inflammation in a mouse model of LPS-induced endotoxemia

Previously, we showed that a myeloid-specific knockout of TRPM7 (*Trpm7 $^{fl/fl}$ LysM Cre*) reduced systemic peripheral inflammation in a mouse model of LPS-induced peritonitis (Schappe et al., 2018). However, the potential of TRPM7 as an immunomodulation target has not been validated through pharmacological approaches. Additionally, since TRPM7 is required for embryogenesis and expressed widely, there have been lingering doubts that drugging TRPM7 would result in systemic toxicity, negating its potential in immunomodulatory therapies. To test whether the in vitro anti-inflammatory properties of VPC4 could extend to in vivo applications, we used a sublethal, LPS-induced peritonitis model for systemic endotoxemia in mice. The experiment would also allow us to address whether high-dose administration of a TRPM7 inhibitor to levels likely to produce channel inhibition in multiple tissues would be tolerable. 12-wk-old WT mice received an intraperitoneal injection with either vehicle, LPS (1 mg/kg), VPC4 (30 mg/kg), or a co-injection of VPC4 and LPS. They were monitored for 4 h for overt pathological symptoms. After 4 h, the mice were euthanized for collection of whole blood and tissues (Fig. 4 A). All mice which received VPC4 achieved whole blood levels that were well above the IC₅₀ for TRPM7 blockade (0.665 μ M), with mean concentrations of 15.78 and 17.35 μ M for the drug-treated and cotreatment groups, respectively (Fig. 4 B). Using an automated hematology analyzer, we measured absolute lymphocyte counts and observed no significant differences between the treatment groups, in line with a previous demonstration that VPC4 does not drive lymphopenia in mice (Zhu et al., 2007; Fig. 4 C). Luminex analysis of plasma cytokines revealed a significant elevation in the levels of inflammatory

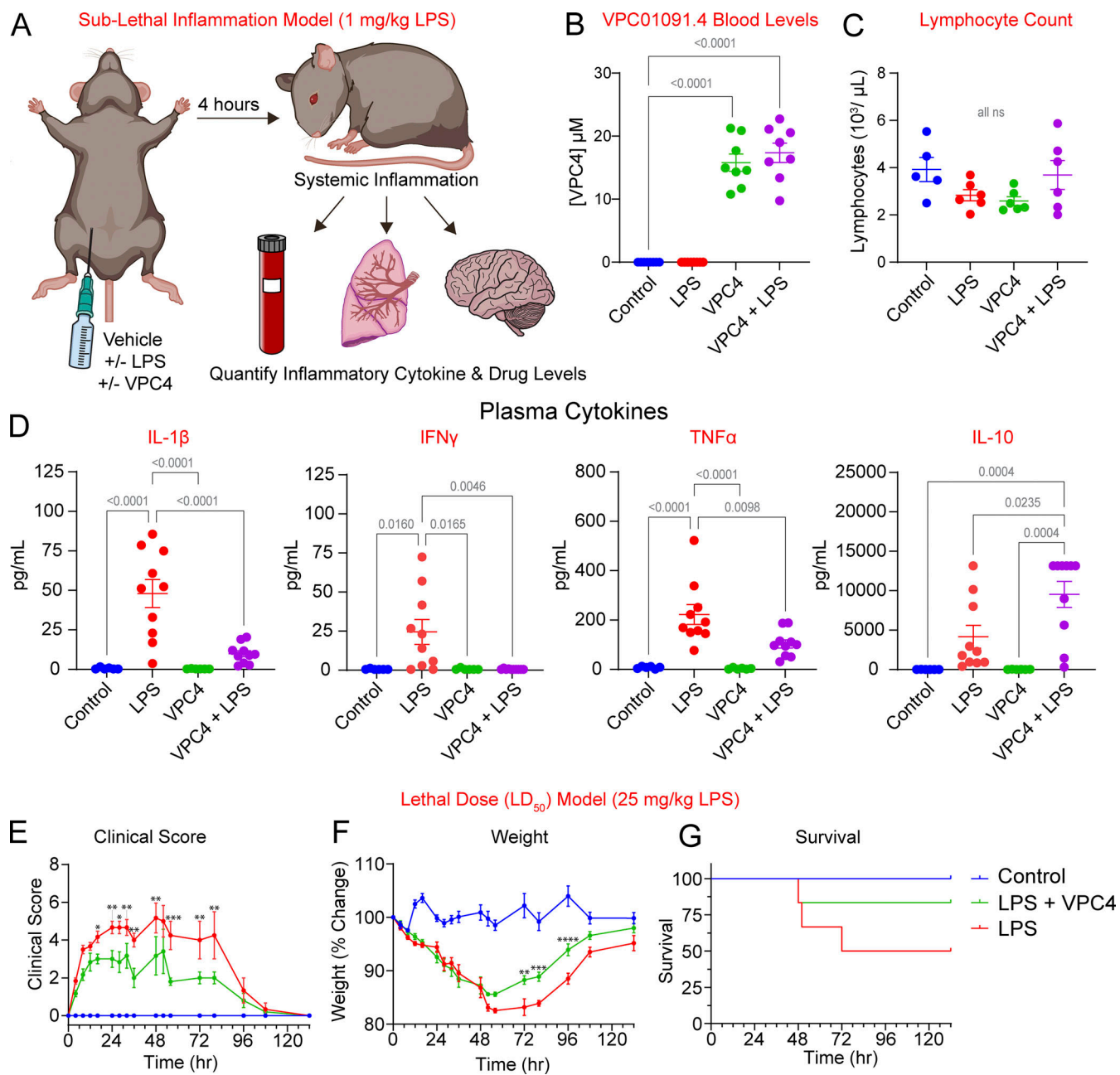


Figure 4. VPC01091.4 suppresses the LPS-induced systemic inflammatory response in vivo. (A) Experiment schematic for the sublethal, LPS-induced inflammation model: 12-wk-old, WT C57BL/6 mice were injected intraperitoneally with LPS (1 mg/kg) with or without coadministered VPC01091.4 (30 mg/kg). After 4 h, mice were euthanized and blood was collected for determination of whole blood drug levels, lymphocyte counts, and plasma cytokine levels. Following biventricular perfusion, lung and brain tissue were collected (see organ data in Fig. 5). (B) Whole-blood levels of VPC01091.4 as determined by LC-MS. Ordinary one-way ANOVA tests were performed for statistical analysis, SEM are shown. (C) Mean lymphocyte counts as determined by an automated hematology analyzer. Ordinary one-way ANOVA tests were performed for statistical analysis, SEM are shown. (D) Plasma cytokines as determined by a Luminex assay for *IL-1 β* , *IFN γ* , *TNF α* , and *IL-10*. Data are pooled from four independently conducted trials with eight mice each ($n = 6$ for control and VPC4-only groups and $n = 10$ for LPS and VPC4 + LPS groups). Ordinary one-way ANOVA tests were performed for statistical analysis, SEM are shown. (E–G) Data from a lethal dose (LD_{50}) LPS model. The experiment was performed similarly to the sublethal model, except mice received an LD_{50} dose of LPS (25 mg/ml), with or without co-administered VPC01091.4 (30 mg/kg); then were monitored for 132 h. Weights and clinical symptoms were measured at each timepoint. (E) Clinical scores over time by treatment group. Significant differences between the LPS and LPS + VPC4 treated groups as determined by a mixed-effects ANOVA analysis are shown (* = $P \leq 0.05$, ** = $P \leq 0.01$, *** = $P \leq 0.001$). (F) Changes in weight from baseline over time by treatment group. Significant differences between the LPS and LPS + VPC4 treated groups as determined by a mixed-effects ANOVA analysis are shown (** = $P \leq 0.01$, *** = $P \leq 0.001$, **** = $P \leq 0.0001$). (G) Kaplan–Meier survival curves by treatment group. The survival rate was 100% for the control group, 50% for the LPS-treated group, and 83.33% for the LPS + VPC4 co-treated group ($n = 6$ mice for each group). A log-rank Mantel–Cox test determined there were no significant differences between treatment groups, with a P value of 0.127.

cytokines *IL-1 β* , *IFN γ* , and *TNF α* in LPS-treated mice. These inflammatory cytokines were significantly suppressed in mice cotreated with LPS and VPC4 (Fig. 4 D). The cotreatment group also demonstrated higher levels of the anti-inflammatory cytokine *IL-10*.

To test whether VPC4 treatment could increase the survival of mice in the setting of LPS-induced endotoxemia, we challenged mice with a 50% lethal dose of LPS and monitored their weight and symptoms for 132 h. The severity of observed conjunctivitis, lethargy, grooming quality, stool changes, and facial grimace were assessed based on standardized scoring parameters (Table 1) to obtain composite clinical scores (Fig. 4 E). Mice that received LPS treatment exclusively had the most severe symptoms, and these symptoms were significantly reduced at a number of timepoints in mice which were cotreated with LPS and VPC4. Control mice displayed no adverse effects at any time points after receiving vehicle treatment. LPS-only and cotreated mice lost weight to a similar degree through the first 48 h of the experiment, at which point the cotreated mice began recovering at a higher nadir and at an earlier timepoint as compared with the LPS-only treated mice (Fig. 4 F). The survival rate of LPS-treated mice was 50% compared with a survival rate of 83.33% in the cotreated mice and 100% in the control mice (Fig. 4 G), though the differences were not statistically significant with a P value of 0.127. At the final timepoint, all mice that had survived the experiment had returned to baseline symptoms with no remaining evidence of toxicity.

Taken together, VPC4 appeared to be well-tolerated and capable of suppressing the systemic inflammatory response produced by intraperitoneal LPS injection without driving lymphopenia. In addition, it reduced the severity of physical symptoms and weight loss in mice challenged with a lethal dose of LPS and produced a non-significant increase in mouse survival.

VPC4 accumulates in the brain and lungs

FTY720 broadly distributes throughout the body, including the central nervous system, and reaches the highest concentration in the lungs (Meno-Tetang et al., 2006). A later study showed more specifically that FTY720 passes through the blood-brain barrier and accumulates in the white matter (Foster et al., 2007). We were hopeful that VPC4 would exhibit similar pharmacological properties and thus prove useful for modulating brain inflammation. Lung and brain tissues collected during our LPS-induced peritonitis model were partitioned, with a portion of the tissue preserved immediately for whole-organ RNA extraction. The remaining tissue was weighed and then mechanically homogenized in PBS with an internal standard (0.5 μ M FTY720). The homogenate was then analyzed by LC-MS. Based on the LC-MS signal intensities of VPC4 and the internal standard (FTY720), the VPC4 concentrations were calculated. In the mice that received VPC4, the VPC4 levels in the brain were approximately ninefold higher than those found in the blood (Fig. 5 A). Lung levels of VPC4 were even higher, reaching 32-fold higher than the blood levels (Fig. 5 C). These results confirm that, like FTY720, VPC4 can pass through the blood-brain barrier. We then evaluated whether VPC4 dampened inflammation in the lung and brain.

VPC4 blunts brain and lung inflammation in the mouse model of endotoxemia

It is well established that peripherally administered endotoxin rapidly induces inflammatory cytokines in the brain (Pitossi et al., 1997; Layé et al., 1994; Gatti and Bartfai, 1993). Whole-tissue RNA was extracted from lung and brain samples and analyzed using qRT-PCR for differences in inflammatory cytokine expression between the treatment groups. Mice treated with LPS had significantly higher brain expression of *IL-1 β* , *IL-6*, *TNF α* , and *CCL4* as compared with control mice, and these cytokines were significantly suppressed through cotreatment with VPC4 (Fig. 5 B). A similar effect was observed in the lung tissue, except for *IL-6*, where the suppression by cotreatment with VPC4 was non-significantly lower than the LPS group (Fig. 5 D). Overall, these findings demonstrate that VPC4 can pass the blood-brain barrier and blunt whole-brain and lung cytokine production during systemic LPS-driven inflammation.

Discussion

Because of their easy accessibility on the cell membrane and rapid switch-like activity that can be locked by small molecules and peptides into ON or OFF states, ion channels are the preferred molecular targets of venoms in nature and many clinical drugs (Wulff et al., 2019). Ion channels expressed by the immune cells are therefore emerging as important targets for immunomodulation (Feske et al., 2015; Froghi et al., 2021). Our previous work has established TRPM7 ion channel activity as a regulator of macrophage-mediated inflammation but a lack of effective small molecule inhibitors that are well-tolerated in vivo prevented pharmacological exploration. This study took advantage of the earlier finding that FTY720, an FDA-approved drug that targets S1P1 for the treatment of multiple sclerosis, inhibits TRPM7 in its unphosphorylated prodrug form, but not in its phosphorylated form. The approach has identified VPC01091.4 (VPC4) and AAL-149 as inhibitors of TRPM7 channel activity. Additionally, we have shown that VPC4 is well-tolerated in mice and has potent anti-inflammatory effects in a mouse model of endotoxemia. Note that even at high doses VPC4 was shown to have no deleterious effect on lymphocyte populations, in line with previous demonstration of its use in vivo (Zhu et al., 2007). A key caveat of these drugs is that, especially at the high doses needed for TRPM7 blockade, off-target effects are a near certainty; underscored by the finding herein that the anti-inflammatory properties are not solely dependent on TRPM7. Nevertheless, these drugs offer the ability to attempt in vivo pharmacologic manipulation of TRPM7, and the potent anti-inflammatory properties are useful even if they result from polypharmacology—both within macrophages and across immune cell populations.

Microglia, the brain-resident macrophages, are major drivers of neuroinflammation, and alleviating neuroinflammation may yield clinical benefit in slowing the progression of many neurodegenerative diseases (Streit et al., 2004; Muzio et al., 2021). Our findings show that VPC4 can inhibit microglial activation ex vivo, pass the blood-brain barrier, and greatly blunt neuroinflammation in an endotoxemia mouse model. In addition to

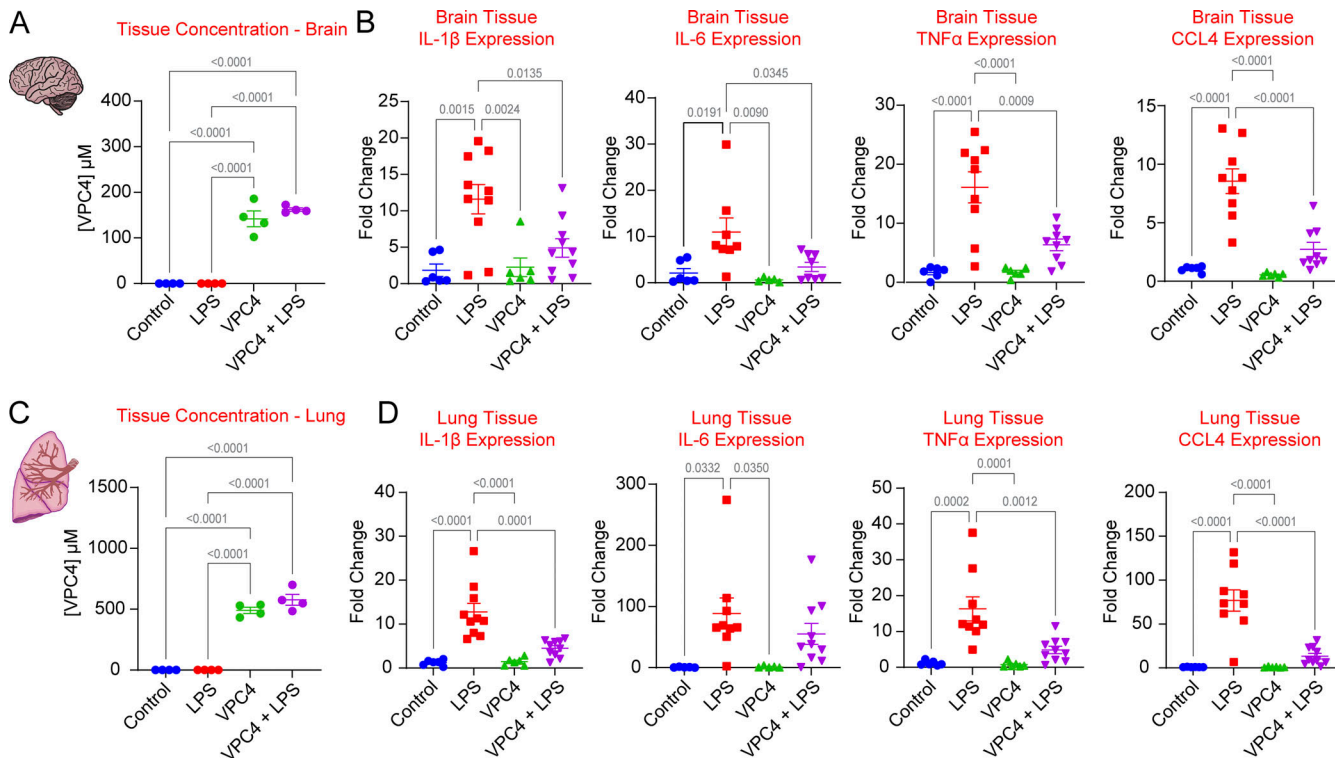


Figure 5. VPC01091.4 crosses the blood–brain barrier and exerts organ-level anti-inflammation in lung and brain tissue. (A) Whole-brain levels of VPC01091.4 as determined by LC-MS. Drug-treated groups had mean brain concentrations of 141.8 μM (VPC4) and 162.2 μM (VPC4 + LPS), 8.97- and 9.35-times higher than mean blood levels, respectively. **(B)** Expression of inflammatory cytokines as measured by qRT-PCR of RNA extracted from whole-brain homogenates. **(C)** Whole-lung levels of VPC01091.4 as determined by LC-MS. Drug-treated groups had mean lung concentrations of 490.3 μM (VPC4) and 576.3 μM (VPC4 + LPS), 31.07- and 33.22-times higher than mean blood levels, respectively. **(D)** Expression of inflammatory cytokines as measured by qRT-PCR of RNA extracted from whole-lung homogenates. Ordinary one-way ANOVA tests were performed for statistical analysis, SEM are shown.

the brain, we show that VPC4 accumulates in the lungs at especially high levels. Alveolar macrophages are the most abundant immune cells in the lung (Cai et al., 2014) and significant drivers of lung immunopathologies such as acute respiratory distress syndrome (Aggarwal et al., 2014). The pharmacokinetic properties observed here suggest that this class of drugs may prove especially useful in targeting inflammatory lung and brain pathologies.

The mechanism through which FTY720 and VPC4 inhibit TRPM7 ion channel activity has not been explored yet. Like many TRP channels, TRPM7 ion channel activity is highly sensitive to interactions with membrane lipids. This was recently reinforced through a structural demonstration that the TRPM7 inhibitors NS8593 and VER155008 stabilize the closed state of TRPM7 by binding to a vanilloid-like pocket that likely interacts with endogenous lipids (Nadezhdin et al., 2023). Sphingosine and FTY720 are not thought to be pore blockers of TRPM7, as they reduce I_{M7} by lowering the open probability without affecting single-channel conductance (Qin et al., 2013). It is therefore possible that sphingosine-like antagonists like FTY720 and VPC4 interfere with the ability of TRPM7 to interact with regulatory phospholipids (Runnels et al., 2001; Kozak et al., 2005). Future structural studies will clarify the underlying mechanisms and facilitate a rational modification of VPC4 for increased potency and selectivity. Thus, this class of non-

phosphorylatable FTY720 analogs represents a fruitful search space for further optimized TRPM7 inhibitors and may lead to a new class of immunomodulatory drugs.

Data availability

All data are available upon reasonable request to the corresponding author (Bimal N. Desai bdesai@virginia.edu).

Acknowledgments

Jeanne M. Nerbonne served as editor.

We would like to thank all members of the Desai and Lynch labs for their scientific insights and feedback. We thank Drs. Kevin Lynch (University of Virginia; UVA), Douglas Bayliss (UVA), Stefanie Redemann (UVA), Norbert Leitinger (UVA), and Mark Beenhakker (UVA) for helpful and timely advice as Thesis Committee advisors to G.W. Busey.

The work was predominantly funded with the following National Institutes of Health research grants: AI155808 (to B.N. Desai), GM108989 (to B.N. Desai), R01AI144026 (to K.R. Lynch), UVA Medical Scientist Training Program Training Grant T32 GM007267 (to G.W. Busey), and UVA Pharmacological Sciences Training Grant T32 GM007055 (to G.W. Busey). The work was also funded with a grant from the Owens Family Foundation (to B.N. Desai).

Open Access funding provided by the VIVA consortium.

Author contributions: Conception: G.W. Busey, K.R. Lynch, and B.N. Desai. Research Design: G.W. Busey and B.N. Desai. Investigation: G.W. Busey, M.C. Manjegowda, T. Huang, W.H. Iobst, S.S. Naphade, J.A. Kennedy, C.A. Doyle, and P.V. Seegren. Data analysis: G.W. Busey, W.H. Iobst, and T. Huang. Resource assistance: K.R. Lynch, B.N. Desai. Writing—Original Draft: G.W. Busey. Writing—Draft and Editing: G.W. Busey, B.N. Desai, K.R. Lynch, M.C. Manjegowda, T. Huang, W.H. Iobst, S.S. Naphade, J.A. Kennedy, C.A. Doyle, and P.V. Seegren. Project Administration: B.N. Desai. The illustrations presented here are original artwork adapted from figures created using <https://Biorender.com>.

Disclosures: K.R. Lynch reported a patent to US 7,754,703 issued. No other disclosures were reported.

Submitted: 22 May 2023

Revised: 4 August 2023

Revised: 25 September 2023

Accepted: 20 October 2023

References

Abiria, S.A., G. Krapivinsky, R. Sah, A.G. Santa-Cruz, D. Chaudhuri, J. Zhang, P. Adstamongkonkul, P.G. DeCaen, and D.E. Clapham. 2017. TRPM7 senses oxidative stress to release Zn²⁺ from unique intracellular vesicles. *Proc. Natl. Acad. Sci. USA.* 114:E6079–E6088. <https://doi.org/10.1073/pnas.1707380114>

Aggarwal, N.R., L.S. King, and F.R. D'Alessio. 2014. Diverse macrophage populations mediate acute lung inflammation and resolution. *Am. J. Physiol. Lung Cell. Mol. Physiol.* 306:L709–L725. <https://doi.org/10.1152/ajplung.00341.2013>

Albert, R., K. Hinterding, V. Brinkmann, D. Guerini, C. Müller-Hartwig, H. Knecht, C. Simeon, M. Streiff, T. Wagner, K. Welzenbach, et al. 2005. Novel immunomodulator FTY720 is phosphorylated in rats and humans to form single stereoisomer. Identification, chemical proof, and biological characterization of the biologically active species and its enantiomer. *J. Med. Chem.* 48:5373–5377. <https://doi.org/10.1021/jm050242f>

Bers, D.M., C.W. Patton, and R. Nuccitelli. 2010. A practical guide to the preparation of Ca(2+) buffers. *Methods Cell Biol.* 99:1–26. <https://doi.org/10.1016/B978-0-12-374841-6.00001-3>

Brinkmann, V., A. Billich, T. Baumrucker, P. Heining, R. Schmouder, G. Francis, S. Aradhya, and P. Burtin. 2010. Fingolimod (FTY720): Discovery and development of an oral drug to treat multiple sclerosis. *Nat. Rev. Drug Discov.* 9:883–897. <https://doi.org/10.1038/nrd3248>

Brinkmann, V., M.D. Davis, C.E. Heise, R. Albert, S. Cottens, R. Hof, C. Bruns, E. Prieschl, T. Baumrucker, P. Hiestand, et al. 2002. The immune modulator FTY720 targets sphingosine 1-phosphate receptors. *J. Biol. Chem.* 277:21453–21457. <https://doi.org/10.1074/jbc.C200176200>

Buehrer, B.M., and R.M. Bell. 1992. Inhibition of sphingosine kinase in vitro and in platelets. Implications for signal transduction pathways. *J. Biol. Chem.* 267:3154–3159. [https://doi.org/10.1016/S0021-9258\(19\)50708-6](https://doi.org/10.1016/S0021-9258(19)50708-6)

Cai, Y., C. Sugimoto, M. Arainga, X. Alvarez, E.S. Didier, and M.J. Kuroda. 2014. In vivo characterization of alveolar and interstitial lung macrophages in rhesus macaques: Implications for understanding lung disease in humans. *J. Immunol.* 192:2821–2829. <https://doi.org/10.4049/jimmunol.1302269>

Camm, J., T. Hla, R. Bakshi, and V. Brinkmann. 2014. Cardiac and vascular effects of fingolimod: Mechanistic basis and clinical implications. *Am. Heart J.* 168:632–644. <https://doi.org/10.1016/j.ahj.2014.06.028>

Chiba, K., Y. Yanagawa, Y. Masubuchi, H. Kataoka, T. Kawaguchi, M. Ohtsuki, and Y. Hoshino. 1998. FTY720, a novel immunosuppressant, induces sequestration of circulating mature lymphocytes by acceleration of lymphocyte homing in rats. I. FTY720 selectively decreases the number of circulating mature lymphocytes by acceleration of lymphocyte homing. *J. Immunol.* 160:5037–5044. <https://doi.org/10.4049/jimmunol.160.10.5037>

Chubanov, V., S. Ferioli, and T. Gudermann. 2017. Assessment of TRPM7 functions by drug-like small molecules. *Cell Calcium.* 67:166–173. <https://doi.org/10.1016/j.ceca.2017.03.004>

Chubanov, V., M. Mederos y Schnitzler, M. Meißner, S. Schäfer, K. Abstiens, T. Hofmann, T. Gudermann, and T. Gudermann. 2012. Natural and synthetic modulators of SK (K^{Ca}2) potassium channels inhibit magnesium-dependent activity of the kinase-coupled cation channel TRPM7. *Br. J. Pharmacol.* 166:1357–1376. <https://doi.org/10.1111/j.1476-5381.2012.01855.x>

Chubanov, V., S. Schäfer, S. Ferioli, and T. Gudermann. 2014. Natural and synthetic modulators of the TRPM7 channel. *Cells.* 3:1089–1101. <https://doi.org/10.3390/cells3041089>

Chubanov, V., S. Waldegg, M. Mederos y Schnitzler, H. Vitzthum, M.C. Sassen, H.W. Seyberth, M. Konrad, and T. Gudermann. 2004. Disruption of TRPM6/TRPM7 complex formation by a mutation in the TRPM6 gene causes hypomagnesemia with secondary hypocalcemia. *Proc. Natl. Acad. Sci. USA.* 101:2894–2899. <https://doi.org/10.1073/pnas.0305252101>

Desai, B.N., G. Krapivinsky, B. Navarro, L. Krapivinsky, B.C. Carter, S. Febyay, M. Delling, A. Penumaka, I.S. Ramsey, Y. Manasian, and D.E. Clapham. 2012. Cleavage of TRPM7 releases the kinase domain from the ion channel and regulates its participation in Fas-induced apoptosis. *Dev. Cell.* 22:1149–1162. <https://doi.org/10.1016/j.devcel.2012.04.006>

Diness, J.G., U.S. Sørensen, J.D. Nissen, B. Al-Shahib, T. Jespersen, M. Grunnet, and R.S. Hansen. 2010. Inhibition of small-conductance Ca²⁺-activated K⁺ channels terminates and protects against atrial fibrillation. *Circ. Arrhythm. Electrophysiol.* 3:380–390. <https://doi.org/10.1161/CIRCEP.110.957407>

Duan, J., Z. Li, J. Li, R.E. Hulse, A. Santa-Cruz, W.C. Valinsky, S.A. Abiria, G. Krapivinsky, J. Zhang, and D.E. Clapham. 2018. Structure of the mammalian TRPM7, a magnesium channel required during embryonic development. *Proc. Natl. Acad. Sci. USA.* 115:E8201–E8210. <https://doi.org/10.1073/pnas.1810719115>

Ferioli, S., S. Zierler, J. Zaifßerer, J. Schredelseker, T. Gudermann, and V. Chubanov. 2017. TRPM6 and TRPM7 differentially contribute to the relief of heteromeric TRPM6/7 channels from inhibition by cytosolic Mg²⁺ and Mg-ATP. *Sci. Rep.* 7:8806. <https://doi.org/10.1038/s41598-017-08144-1>

Feske, S., H. Wulff, and E.Y. Skolnik. 2015. Ion channels in innate and adaptive immunity. *Annu. Rev. Immunol.* 33:291–353. <https://doi.org/10.1146/annurev-immunol-032414-112212>

Foster, C.A., L.M. Howard, A. Schweitzer, E. Persohn, P.C. Hiestand, B. Balaton, R. Reuschel, C. Beerli, M. Schwartz, and A. Billich. 2007. Brain penetration of the oral immunomodulatory drug FTY720 and its phosphorylation in the central nervous system during experimental autoimmune encephalomyelitis: Consequences for mode of action in multiple sclerosis. *J. Pharmacol. Exp. Ther.* 323:469–475. <https://doi.org/10.1124/jpet.107.127183>

Freij, C., A. Andersson, B. Larsson, L.J. Guo, E. Norström, K.E. Happonen, and B. Dahlbäck. 2015. Quantification of sphingosine 1-phosphate by validated LC-MS/MS method revealing strong correlation with apolipoprotein M in plasma but not in serum due to platelet activation during blood coagulation. *Anal. Bioanal. Chem.* 407:8533–8542. <https://doi.org/10.1007/s00216-015-9008-4>

Froghi, S., C.R. Grant, R. Tandon, A. Quaglia, B. Davidson, and B. Fuller. 2021. New insights on the role of TRP channels in calcium signalling and immunomodulation: Review of pathways and implications for clinical practice. *Clin. Rev. Allergy Immunol.* 60:271–292. <https://doi.org/10.1007/s12016-020-08824-3>

Gatti, S., and T. Bartfai. 1993. Induction of tumor necrosis factor-alpha mRNA in the brain after peripheral endotoxin treatment: Comparison with interleukin-1 family and interleukin-6. *Brain Res.* 624:291–294. [https://doi.org/10.1016/0006-8993\(93\)90090-A](https://doi.org/10.1016/0006-8993(93)90090-A)

Groenestegge, W.M., J.G. Hoenderop, L. van den Heuvel, N. Knoers, and R.J. Bindels. 2006. The epithelial Mg²⁺ channel transient receptor potential melastatin 6 is regulated by dietary Mg²⁺ content and estrogens. *J. Am. Soc. Nephrol.* 17:1035–1043. <https://doi.org/10.1681/ASN.2005070700>

Heng, T.S.P., M.W. Painter, K. Elpek, V. Lukacs-Kornek, N. Mauermann, S.J. Turley, D. Koller, F.S. Kim, A.J. Wagers, N. Asinovski, et al. 2008. The immunological genome Project: Networks of gene expression in immune cells. *Nat. Immunol.* 9:1091–1094. <https://doi.org/10.1038/ni008-1091>

Jin, J., B.N. Desai, B. Navarro, A. Donovan, N.C. Andrews, and D.E. Clapham. 2008. Deletion of Trpm7 disrupts embryonic development and

thymopoiesis without altering Mg²⁺ homeostasis. *Science*. 322:756–760. <https://doi.org/10.1126/science.1163493>

Jin, J., L.J. Wu, J. Jun, X. Cheng, H. Xu, N.C. Andrews, and D.E. Clapham. 2012. The channel kinase, TRPM7, is required for early embryonic development. *Proc. Natl. Acad. Sci. USA*. 109:E225–E233. <https://doi.org/10.1073/pnas.1120033109>

Koivisto, A.-P., M.G. Belvisi, R. Gaudet, and A. Szallasi. 2022. Advances in TRP channel drug discovery: From target validation to clinical studies. *Nat. Rev. Drug Discov.* 21:41–59. <https://doi.org/10.1038/s41573-021-00268-4>

Kozak, J.A., M. Matsushita, A.C. Nairn, and M.D. Cahalan. 2005. Charge screening by internal pH and polyvalent cations as a mechanism for activation, inhibition, and rundown of TRPM7/MIC channels. *J. Gen. Physiol.* 126:499–514. <https://doi.org/10.1085/jgp.200509324>

Layé, S., P. Parnet, E. Goujon, and R. Dantzer. 1994. Peripheral administration of lipopolysaccharide induces the expression of cytokine transcripts in the brain and pituitary of mice. *Brain Res. Mol. Brain Res.* 27:157–162. [https://doi.org/10.1016/0169-328X\(94\)90197-X](https://doi.org/10.1016/0169-328X(94)90197-X)

Lynch, K. and T. Macdonald. 2006. Sphingosine 1-phosphate agonists comprising cycloalkanes and 5-membered heterocycles substituted by amino and phenyl groups. *WO2006088944*, August 24.

Matloubian, M., C.G. Lo, G. Cinamon, M.J. Lesneski, Y. Xu, V. Brinkmann, M.L. Allende, R.L. Proia, and J.G. Cyster. 2004. Lymphocyte egress from thymus and peripheral lymphoid organs is dependent on S1P receptor 1. *Nature*. 427:355–360. <https://doi.org/10.1038/nature02284>

Mendu, S.K., M.E. Stremska, M.S. Schappe, E.K. Moser, J.K. Krupa, J.S. Rogers, E.J. Stipes, C.A. Parker, T.J. Braciele, J.S.A. Perry, and B.N. Desai. 2020. Targeting the ion channel TRPM7 promotes the thymic development of regulatory T cells by promoting IL-2 signaling. *Sci. Signal.* 13: eabb0619. <https://doi.org/10.1126/scisignal.abb0619>

Meno-Tetang, G.M.L., H. Li, S. Mis, N. Pyszczynski, P. Heinig, P. Lowe, and W.J. Jusko. 2006. Physiologically based pharmacokinetic modeling of FTY720 (2-amino-2[2-(4-octylphenyl)ethyl]propane-1,3-diol hydrochloride) in rats after oral and intravenous doses. *Drug Metab. Dispos.* 34:1480–1487. <https://doi.org/10.1124/dmd.105.009001>

Merrill, A.H., Jr. 2002. De novo sphingolipid biosynthesis: A necessary, but dangerous, pathway. *J. Biol. Chem.* 277:25843–25846. <https://doi.org/10.1074/jbc.R200009200>

Moran, M.M. 2018. TRP channels as potential drug targets. *Annu. Rev. Pharmacol. Toxicol.* 58:309–330. <https://doi.org/10.1146/annurev-pharmtox-010617-052832>

Muzio, L., A. Viotti, and G. Martino. 2021. Microglia in neuroinflammation and neurodegeneration: From understanding to therapy. *Front. Neurosci.* 15:742065. <https://doi.org/10.3389/fnins.2021.742065>

Nadezhdin, K.D., L. Correia, C. Narangoda, D.S. Patel, A. Neuberger, T. Gudermann, M.G. Kurnikova, V. Chubanov, and A.I. Sobolevsky. 2023. Structural mechanisms of TRPM7 activation and inhibition. *Nat. Commun.* 14:2639. <https://doi.org/10.1038/s41467-023-38362-3>

Nadler, M.J.S., M.C. Hermosura, K. Inabe, A.-L. Perraud, Q. Zhu, A.J. Stokes, T. Kuroski, J.-P. Kinet, R. Penner, A.M. Scharenberg, and A. Fleig. 2001. LTRPC7 is a Mg,ATP-regulated divalent cation channel required for cell viability. *Nature*. 411:590–595. <https://doi.org/10.1038/35079092>

Nayak, D.K., O. Mendez, S. Bowen, and T. Mohanakumar. 2018. Isolation and in vitro culture of murine and human alveolar macrophages. *J. Vis. Exp.* 57:287. <https://doi.org/10.3791/57287>

Oancea, E., J.T. Wolfe, and D.E. Clapham. 2006. Functional TRPM7 channels accumulate at the plasma membrane in response to fluid flow. *Circ. Res.* 98:245–253. <https://doi.org/10.1161/01.RES.0000200179.29375.cc>

Paugh, S.W., S.G. Payne, S.E. Barbour, S. Milstien, and S. Spiegel. 2003. The immunosuppressant FTY720 is phosphorylated by sphingosine kinase type 2. *FEBS Lett.* 554:189–193. [https://doi.org/10.1016/S0014-5793\(03\)01168-2](https://doi.org/10.1016/S0014-5793(03)01168-2)

Pitossi, F., A. del Rey, A. Kabiersch, and H. Besedovsky. 1997. Induction of cytokine transcripts in the central nervous system and pituitary following peripheral administration of endotoxin to mice. *J. Neurosci. Res.* 48: 287–298. [https://doi.org/10.1002/\(SICI\)1097-4547\(19970515\)48:4<287::AID-JNR1>3.0.CO;2-7](https://doi.org/10.1002/(SICI)1097-4547(19970515)48:4<287::AID-JNR1>3.0.CO;2-7)

Qin, X., Z. Yue, B. Sun, W. Yang, J. Xie, E. Ni, Y. Feng, R. Mahmood, Y. Zhang, and L. Yue. 2013. Sphingosine and FTY720 are potent inhibitors of the transient receptor potential melastatin 7 (TRPM7) channels. *Br. J. Pharmacol.* 168:1294–1312. <https://doi.org/10.1111/bph.12012>

Runnels, L.W., L. Yue, and D.E. Clapham. 2001. TRP-PLIK, a bifunctional protein with kinase and ion channel activities. *Science*. 291:1043–1047. <https://doi.org/10.1126/science.1058519>

Sanna, M.G., J. Liao, E. Jo, C. Alfonso, M.Y. Ahn, M.S. Peterson, B. Webb, S. Lefebvre, J. Chun, N. Gray, and H. Rosen. 2004. Sphingosine 1-phosphate (S1P) receptor subtypes S1P1 and S1P3, respectively, regulate lymphocyte recirculation and heart rate. *J. Biol. Chem.* 279: 13839–13848. <https://doi.org/10.1074/jbc.M311743200>

Schappe, M.S., M.E. Stremska, G.W. Busey, T.K. Downs, P.V. Seegren, S.K. Mendu, Z. Flegal, C.A. Doyle, E.J. Stipes, and B.N. Desai. 2022. Efferocytosis requires periphagosomal Ca²⁺-signaling and TRPM7-mediated electrical activity. *Nat. Commun.* 13:3230. <https://doi.org/10.1038/s41467-022-30959-4>

Schappe, M.S., K. Szteyn, M.E. Stremska, S.K. Mendu, T.K. Downs, P.V. Seegren, M.A. Mahoney, S. Dixit, J.K. Krupa, E.J. Stipes, et al. 2018. Chanzyme TRPM7 mediates the Ca²⁺ influx essential for lipopolysaccharide-induced toll-like receptor 4 endocytosis and macrophage activation. *Immunity*. 48:59–74.e5. <https://doi.org/10.1016/j.jimmuni.2017.11.026>

Shaner, R.L., J.C. Allegood, H. Park, E. Wang, S. Kelly, C.A. Haynes, M.C. Sullards, and A.H. Merrill Jr. 2009. Quantitative analysis of sphingolipids for lipidomics using triple quadrupole and quadrupole linear ion trap mass spectrometers. *J. Lipid Res.* 50:1692–1707. <https://doi.org/10.1194/jlr.D800051-JLR200>

Steinborn, C., T. Huber, J. Lichtenegger, I. Plangger, K. Wurst, and T. Magauer. 2023. Total syntheses of (+)-Waixenincin A, (+)-9-Deacetoxyl-14,15-depoxyxenicalin, and (-)-Xeniafarauanol A. *J. Am. Chem. Soc.* 145: 11811–11817. <https://doi.org/10.1021/jacs.3c03366>

Streit, W.J., R.E. Mrak, and W.S.T. Griffin. 2004. Microglia and neuroinflammation: A pathological perspective. *J. Neuroinflammation*. 1:14. <https://doi.org/10.1186/1742-2094-1-14>

Strøbaek, D., C. Hougaard, T.H. Johansen, U.S. Sørensen, E.Ø. Nielsen, K.S. Nielsen, R.D.T. Taylor, P. Pedarzani, and P. Christophersen. 2006. Inhibitory gating modulation of small conductance Ca²⁺-activated K⁺ channels by the synthetic compound (R)-N-(benzimidazol-2-yl)-1,2,3,4-tetrahydro-1-naphthylamine (NS8593) reduces afterhyperpolarizing current in hippocampal CA1 neurons. *Mol. Pharmacol.* 70:1771–1782. <https://doi.org/10.1124/mol.106.027110>

Sun, H.-S., F.D. Horgen, D. Romo, K.G. Hull, S.A. Kiledal, A. Fleig, and Z.-P. Feng. 2020. Waixenincin A, a marine-derived TRPM7 inhibitor: A promising CNS drug lead. *Acta Pharmacol. Sin.* 41:1519–1524. <https://doi.org/10.1038/s41401-020-00512-4>

Turlova, E., R. Wong, B. Xu, F. Li, L. Du, S. Habbous, F.D. Horgen, A. Fleig, Z.-P. Feng, and H.-S. Sun. 2021. TRPM7 mediates neuronal cell death upstream of calcium/calmodulin-dependent protein kinase II and calcineurin mechanism in neonatal hypoxic-ischemic brain injury. *Transl. Stroke Res.* 12:164–184. <https://doi.org/10.1007/s12975-020-00810-3>

Wulff, H., P. Christophersen, P. Colussi, K.G. Chandy, and V. Yarov-Yarovoy. 2019. Antibodies and venom peptides: New modalities for ion channels. *Nat. Rev. Drug Discov.* 18:339–357. <https://doi.org/10.1038/s41573-019-0013-8>

Zhu, R., A.H. Snyder, Y. Kharel, L. Schaffter, Q. Sun, P.C. Kennedy, K.R. Lynch, and T.L. Macdonald. 2007. Asymmetric synthesis of conformationally constrained fingolimod analogues--discovery of an orally active sphingosine 1-phosphate receptor type-1 agonist and receptor type-3 antagonist. *J. Med. Chem.* 50:6428–6435. <https://doi.org/10.1021/jm7010172>

Zierler, S., G. Yao, Z. Zhang, W.C. Kuo, P. Pörzgen, R. Penner, F.D. Horgen, and A. Fleig. 2011. Waixenincin A inhibits cell proliferation through magnesium-dependent block of transient receptor potential melastatin 7 (TRPM7) channels. *J. Biol. Chem.* 286:39328–39335. <https://doi.org/10.1074/jbc.M111.264341>

Supplemental material

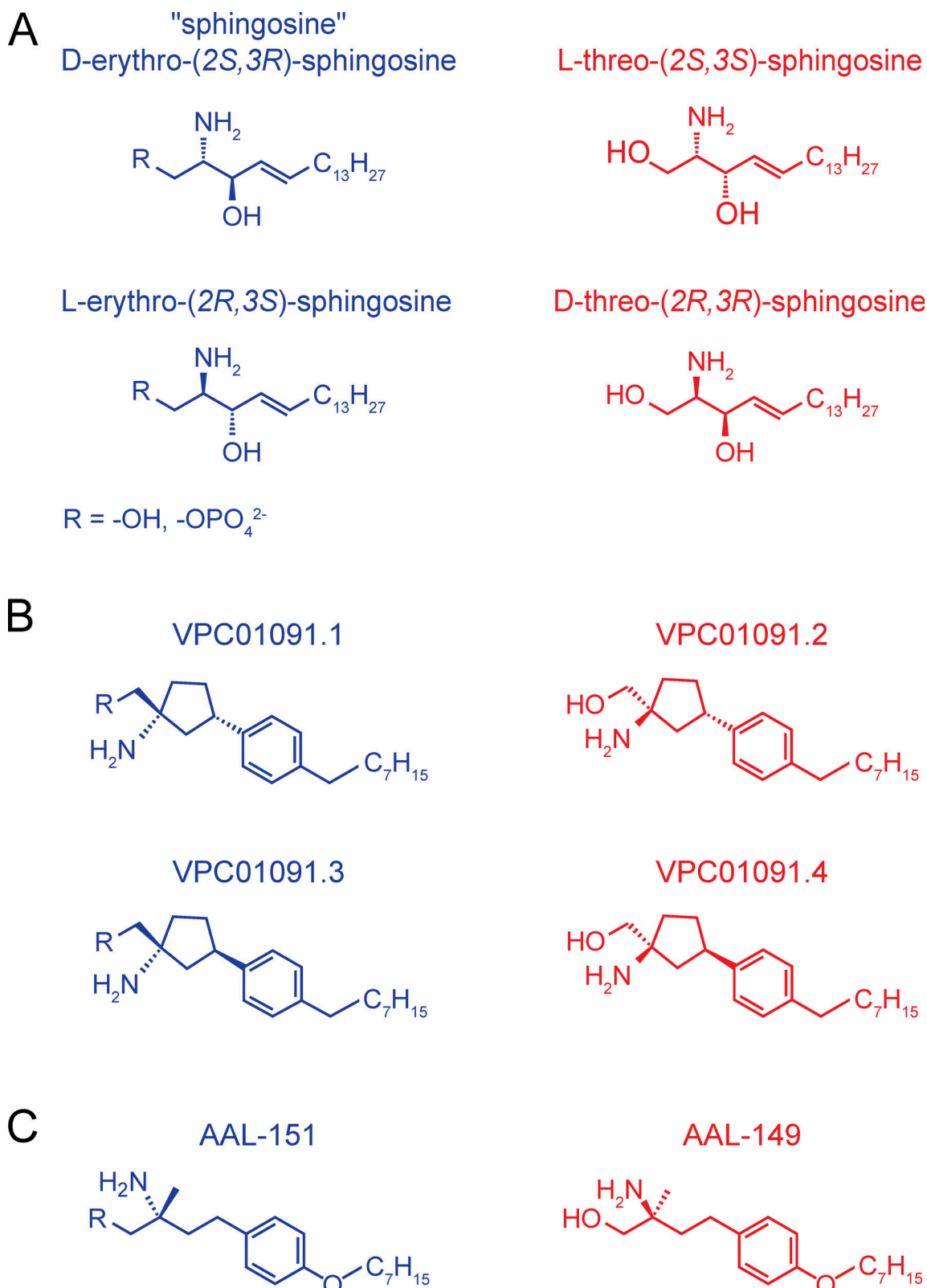


Figure S1. Stereoisomers of sphingosine, VPC01091, and AAL-149. (A) There are four stereoisomers of sphingosine, only D-erythro-sphingosine occurs naturally. The erythro-isomers are substrates for sphingosine kinases and are capable of being phosphorylated in vivo. In contrast, the threo-isomers both act as competitive inhibitors of sphingosine kinases and are not appreciably phosphorylated in vivo. Phosphorylatable isomers are shown in blue. (B) The four diastereomers of VPC01091 are shown. VPC01091.1 and VPC01091.3 (blue) are substrates for sphingosine kinases, whereas VPC01091.2 and VPC01091.4 (red) are not. All four stereoisomers can be chemically phosphorylated, such as with VPC01091.2-phosphate used in the present study. (C) AAL-149 and its phosphorylatable enantiomer, AAL-151, are shown.

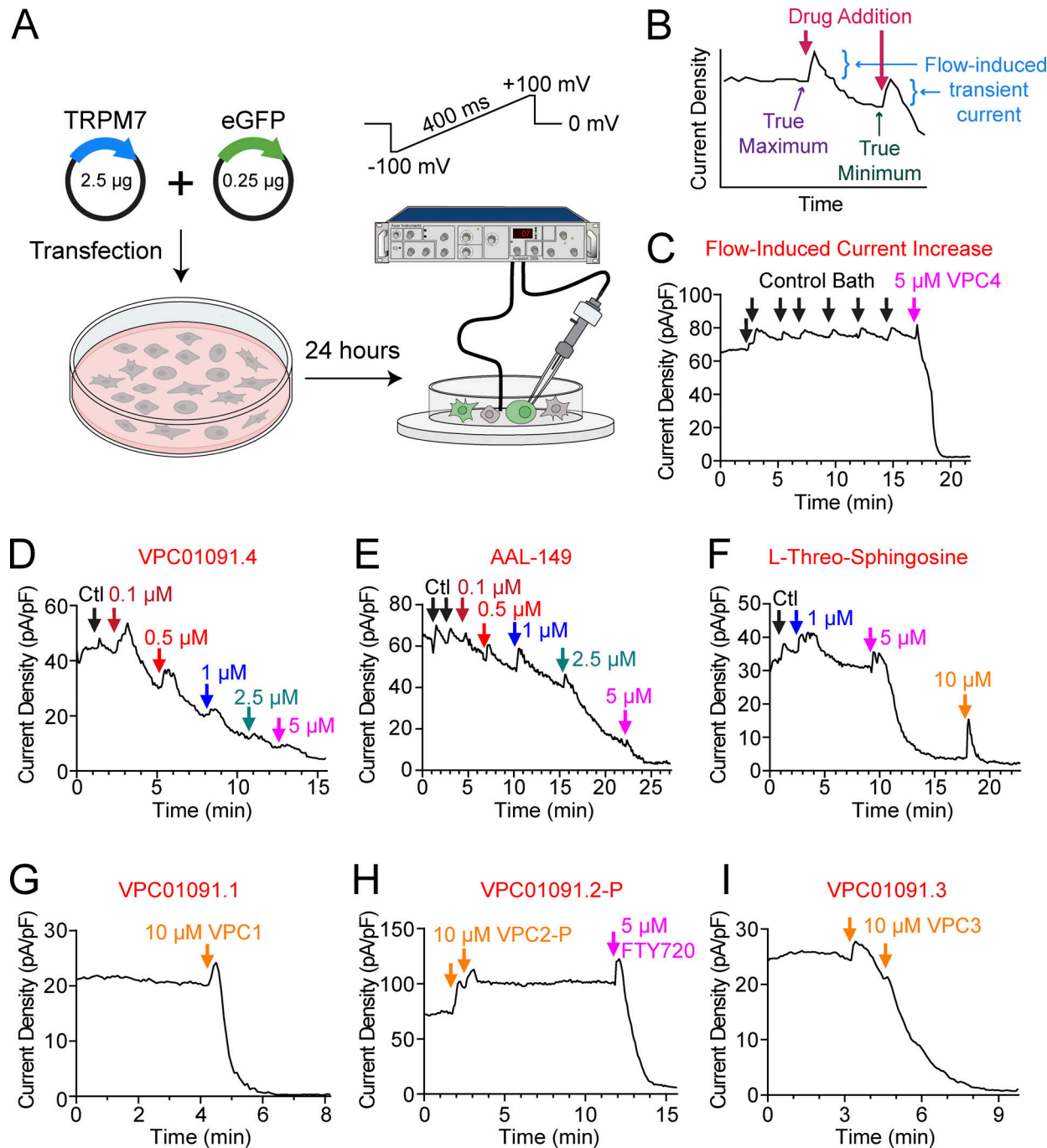


Figure S2. VPC01091.4, AAL-149, and L-threo-sphingosine inhibit TRPM7 current. (A) Schematic depicting the experimental setup for recording whole-cell currents of overexpressed mouse TRPM7 from HEK 293T cells. HEK 293T cells were transfected with a 10:1 ratio of WT mouse TRPM7 and eGFP using jetOptimus transfection reagent. After 24 h, recordings were obtained from GFP-positive cells using an Axopatch 200b amplifier with a 400 ms ramp from -100 to +100 mV and a holding potential of 0 mV. **(B)** Schematic depicting the interpretation of peak current density at +100 mV versus time graphs. The perfusion of bath solution produces a flow-induced transient current increase (shown in blue). The current observed prior to the flow-induced transient is taken as the true maximum current. The trough observed after the decay of the flow-induced transient and prior to the next dose of inhibitory drug is taken as the true minimum current. The fraction of current remaining for each drug dose is taken as the local minimum current over the true maximum current for the recording. **(C)** Example TRPM7 current density at +100 mV versus time graph for a recording in which control bath is repeatedly added to the recording chamber. Each addition of control bath produces a flow-induced transient current that decays back towards the pre-infusion maximum. Later addition of 5 µM VPC01091.4 leads to current inhibition. **(D)** Example TRPM7 current density at +100 mV versus time graph for increasing concentrations of VPC01091.4. Arrows depict the time at which the recording solution was replaced with control solution or VPC01091.4 at the indicated concentration. **(E)** Example TRPM7 current density at +100 mV versus time graph for increasing concentrations of AAL-149. **(F)** Example TRPM7 current density at +100 mV versus time graph for increasing concentrations of L-threo-sphingosine. **(G-I)** Example TRPM7 current density at +100 mV versus time graphs for VPC01091 stereoisomers. Application of 10 µM VPC01091.1 (G) or VPC01091.3 (I) leads to current inhibition. Application of 10 µM VPC01091.2-P (H) does not lead to current inhibition, but the current is later blocked through the addition of 5 µM FTY720.